Dynamic Resistance Probe for the Measurement of the Mass Deposition Rate from a Condensible Propellant Thruster (updated July 2015)

IEPC-2015-199/ISTS-2015-b-199

Presented at Joint Conference of 30th International Symposium on Space Technology and Science, 34th International Electric Propulsion Conference and 6th Nano-satellite Symposium
Hyogo-Kobe, Japan
July 4–10, 2015

William J. Coogan*, Michael A. Hepler†, and Edgar Y. Choueiri‡
Electric Propulsion and Plasma Dynamics Lab
Princeton University, Princeton, NJ, 08544, USA

A new diagnostic for measuring condensible propellant deposition, the dynamic resistance probe, is presented. Using Ohm's law, a theory is formulated to model the rate of lithium deposition as a function of the voltage and temperature of the probe over a given time period. A proof-of-concept experiment is performed on a lithium Lorentz force accelerator which validates the theoretical model, measuring a lithium mass flux of 0.35 µg/cm^2 s with a 95% confidence bound at 6% of the measurement.

Nomenclature

A = area of plume at a given radius from thruster
B_A = applied field strength
d = distance from anode exit plane to point of measurement
g_0 = sea-level gravitational acceleration
h_{Li} = accumulated thickness of lithium on DRP
h_{SS} = thickness of DRP
I = current through DRP
J = current through thruster electrodes
l = length of DRP
$\dot{m}$ = mass flow rate
r_a = anode radius
r_c = cathode radius
R_{Li} = resistance of lithium film
R_{SS} = resistance of 304 stainless steel
t = time
t_c = time correction term
T = temperature
v = velocity of lithium on probe surface due to gravity
V = voltage measured across DRP
w = width of DRP

*Graduate Student, MAE Dept., wcoogan@princeton.edu
†Graduate Student, MAE Dept., mhepler@princeton.edu
‡Chief Scientist, EPPDyL, Professor, Applied Physics Group, MAE Dept., choueiri@princeton.edu

x = distance from end of cathode to end of anode
z = direction perpendicular to the coated surface of DRP
Γ = propellant mass flux through probe surface
Γ_{drip} = propellant mass flux off of probe surface due to gravity
$\bar{\Gamma}$ = ratio of mass flux off of probe to mass flux onto probe
θ = angle of plume divergence from center axis
μ = dynamic viscosity
ρ_{Li} = resistivity of lithium
ρ_{SS} = resistivity of 304 stainless steel
ϱ = density of lithium
τ = total duration of mass deposition
ϕ = angle between DRP and the plane normal to gravity

I. Introduction

A significant concern facing plasma thrusters using applied magnetic fields is the possibility of charged particles attached to the field lines traveling upstream of the solenoid and damaging the spacecraft. The extent to which this behavior occurs has yet to be fully characterized. The effect is difficult to quantify in a laboratory environment because of the size of typical vacuum facilities, which results in reflected propellant particles reaching the region upstream of the thruster along with the particles following the magnetic field lines, artificially increasing the measured mass flux. This upstream region also presents measurement difficulties due to the small flux of ionized particles and the noise generated by proximity to the thruster arc, resulting in a poor signal-to-noise ratio in Faraday probes or retarding potential analyzers (RPAs).[1]

The reflection of particles can be partially mitigated by using condensible propellants. Although backscattering off the vacuum chamber walls cannot be neglected,[2] the condensation of the propellant on the vacuum chamber walls results in lower background pressure by an order of magnitude or more,[3] and therefore fewer reflected particles upstream of the thruster.

Despite the advantage of reduced background pressure, condensible propellants are disadvantageous in that they coat diagnostics exposed to the plume. This is problematic for Langmuir probes, which require we know the changing area of the probe as the propellant accumulates. It is also a problem for RPAs, which require multiple potentials on conducting grids. If a conductive condensible propellant is used, these grids can be bridged by the propellant, bringing them to the same potential.

One diagnostic, the Quartz Crystal Microbalance (QCM) has already shown some promise in measuring the mass flux of condensible propellants.[2] The QCM works by using the accumulation of propellant to damp the vibration of a quartz crystal. The deposition rate can be obtained from the resulting change in vibrational frequency. Although the QCM has been implemented successfully to measure mass fluxes of teflon from a pulsed plasma thruster[2] and molybdenum from an ion thruster,[5] there are some difficulties utilizing a QCM with high power thrusters, such as applied-field magnetoplasmadynamic thrusters (AF-MPDTs). QCMs are very sensitive to temperature changes, and only operate reliably up to 130° C. This limitation can be mitigated with active cooling as well as with the use of a shutter to limit exposure of the probe to the plume. Even with both of these apparatuses in place, Krämer's measurements[10] of the mass flux from the lithium Lorentz force accelerator (LiLFA), an AF-MPDT using lithium propellant, had errors that were approximately 20% of the measurement at 2 µg/cm^2 s, which he attributed to noise from the current discharged through the thruster.

Another technique for measuring the mass deposition rate on a surface is to simply measure the mass on a surface before and after firing. This method can reliably determine the average mass flux, but for this average deposition rate to be representative of the instantaneous value, only a single set of operating parameters (B_A, J, $\dot{m}$, etc.) can be used while firing since the measurement is not time-resolved. Using one set of parameters per firing is prohibitively time consuming, as preparation and cleanup for use of some condensible propellants, such as lithium, requires several days for a single firing. Further, as will be shown in the data presented in Sec. IV, when a thruster first fires, the deposition rate changes while the thruster reaches steady state, so the average mass flux will differ from the steady state mass flux.

The Dynamic Resistance Probe (DRP) is a new type of diagnostic that takes advantage of the deposition

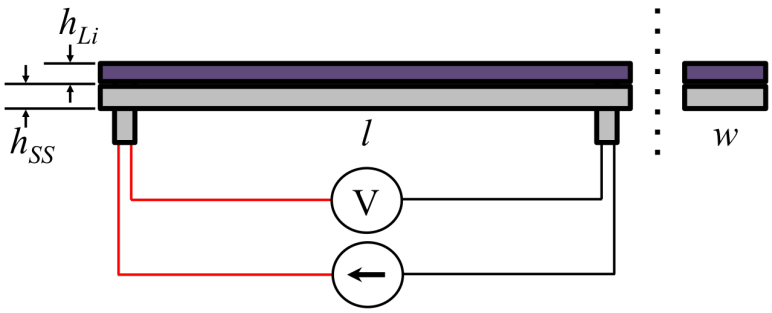

Figure 1. Left: side view of the DRP. The bottom half is 304 stainless steel and of constant dimensions. The top half is a film of lithium propellant of equal area, but variable height. A constant current is run through the probe and the potential is measured across the probe lengthwise. Right: end view of the DRP.

of conducting propellant and provides a measurement of the instantaneous deposition rate. It has the capability of measuring changes in the mass deposition rate during a single firing. It also has the potential to measure the low rates of deposition upstream of a thruster using an applied field as well as the plume divergence downstream. In the following section, we outline the theory of operation using lithium as an example propellant, along with expected sources of error and methods for mitigating error. Then, in Sec. III, we describe the facilities in which the DRP is first tested, as well as the characteristics of the probe. Finally, in Sec. IV, the results of the first experiment using a DRP to measure propellant deposition from a lithium Lorentz force accelerator are presented.

II. Dynamic Resistance Probe Theory

In principle, the DRP works similarly to an ohmmeter. It is a stainless steel band, through which a constant current is conducted. As the steel is coated with lithium, the resistance between the ends of the probe decreases and a corresponding decrease in potential is measured. A diagram of the probe is shown in Fig. 1. The mathematical relation which defines the potential across the probe, V, is the simplified Ohm's law with two resistors in parallel:

$$V = I\left(\frac{R_{SS}R_{Li}}{R_{SS}+R_{Li}}\right). \tag{1}$$

Here, I is the current through the probe, R_{SS} is the resistance of the stainless steel band, and R_{Li} is the resistance of the lithium film.

The resistance of the stainless steel band is

$$R_{SS} = \frac{\rho_{SS} l}{w h_{SS}}, \tag{2}$$

which is calculated from the resistivity of the steel, ρ_{SS}, and both the length, l, and cross-sectional area, wh_{SS}, of the band. Making the assumption that the lithium is evenly distributed over the surface of the probe, the thickness of the lithium coating,

$$h_{Li} = \frac{\Gamma t}{\varrho}, \tag{3}$$

where Γ is the propellant mass flux, t is time, and ϱ is the mass density of lithium. The resistance of lithium is then

$$R_{Li} = \frac{\rho_{Li} l \varrho}{w \Gamma t}. \tag{4}$$

The resistivities of both stainless steel and lithium have a strong temperature dependence, which also needs to be modeled. The resistivity of lithium is found in Ref. [8] to be described by

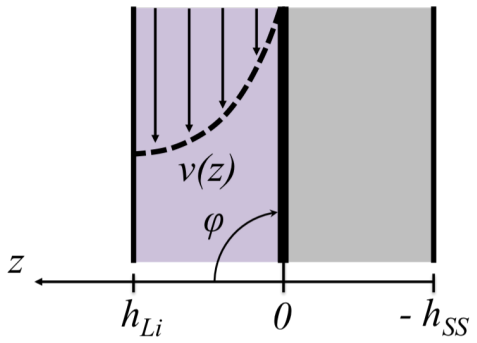

Figure 2. Diagram illustrating how the velocity of lithium flow along the DRP, v, changes as a function of z. h_{Li} is the thickness of the lithium coating the band. h_{SS} is the thickness of the probe.

$$\log(\rho_{Li}(T)\times 10^8) = \begin{cases} 0.1575 + 2.314\log\left(\frac{T}{93.3}\right) - 1.962\log\left(\frac{T}{93.3}\right)^2 + 1.127\log\left(\frac{T}{93.3}\right)^3, & 93.3 < T < 453.6, \\ 1.395 + 0.622\log\left(\frac{T}{453.7}\right) - 0.228\log\left(\frac{T}{453.7}\right)^2 + 0.430\log\left(\frac{T}{453.7}\right)^3, & 453.7 < T < 1080.5, \end{cases} \tag{5}$$

where T is the temperature in K. This equation is based on least mean square fits to 21 independent data sets below 453.7 K (the melting point of lithium), and 17 data sets above that temperature.

Similarly, Ref. [9] lists data points for the resistivity of 304 stainless steel throughout the temperature range of interest (293-1500 K), which can be fit with a polynomial of the form

$$\rho_{SS}(T) = 10^{-16}\,T^3 - 6\times 10^{-13}\,T^2 - 10^{-9}\,T + 4\times 10^{-7}. \tag{6}$$

Finally, we can rearrange Eqs. 1, 2, and 4 to express the mass flux across the surface of the probe:

$$\Gamma = \frac{\rho_{Li}(T)\varrho\,[Il\rho_{SS}(T) - Vwh_{SS}]}{\rho_{SS}(T)wVt}. \tag{7}$$

A. Normalized Criterion for Negligible Dripping

If a probe is close enough to the thruster, lithium will remain liquid on its surface. It is assumed that a liquid lithium film will flow off of the probe, making the probe's operation suboptimal and challenging to characterize. It is important to determine the impact of this drip effect in order to know where and for how long the DRP can be a useful tool. As depicted in Fig. 2, it is assumed that there is a no-slip condition between the lithium and the steel. The velocity of the lithium along the probe, v, increases as a function of distance, z, from the probe, and is therefore a maximum at the surface where $z = h_{Li}$. It is also assumed that the impinging plume has a negligible shear on the lithium surface. It can be shown[12] that for a liquid film of constant thickness, h_{Li},

$$v(h_{Li}) = \frac{\varrho g_0 h_{Li}^2 \sin(\phi)}{2\mu}. \tag{8}$$

ϕ is the angle between the probe and the plane perpendicular to the direction of gravity, and μ is the dynamic viscosity of the liquid.

The dynamic viscosity of lithium is dependent on temperature. Using a table of values for μ from Ref. [11], a power fit is made to create an expression for μ (Pa s) as a function of temperature, T (K), given by

$$\mu = 0.161T^{-0.929}. \tag{9}$$

This expression for μ can now be substituted into the expression for the maximum flow velocity along with our previous expression for h_{Li}. In this instance, the probe is parallel to the direction of gravity, so $\phi = 90°$. Further, the maximum velocity can be nondimensionalized by multiplying by time and dividing

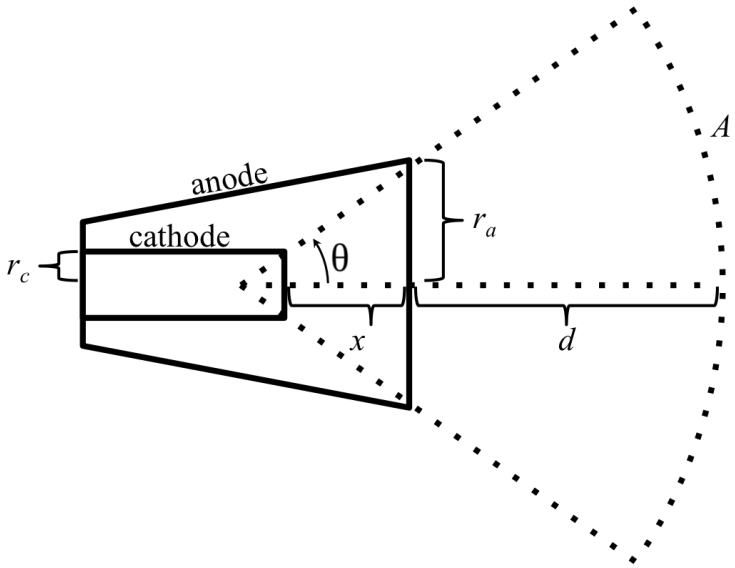

Figure 3. Cross-sectional diagram of the lithium Lorentz force accelerator.

by the length of the probe. By using the duration of the experiment, τ, as the characteristic time scale, an upper bound for the ratio, $\bar{\Gamma}$, of mass flux off the probe compared to the mass flux onto the probe is found:

$$\bar{\Gamma} = \frac{\Gamma_{\text{drip}}}{\Gamma} = \frac{\varrho g_0 h_{Li}(\tau)\tau \sin(\phi)}{2\mu}. \tag{10}$$

It is desired that $\bar{\Gamma}$ be $\ll 1$ for effects of lithium being removed from our probe to be negligible. Otherwise, the probe must either be moved to a distance from the thruster where the temperature is below the melting temperature of lithium, or the probe must be actively cooled.

B. Approximation of Lithium Mass Flux

In order to anticipate an approximate mass flux of lithium across the probe, we make simplifying assumptions as previously proposed by Krämer.[10] The deposition is assumed to be evenly distributed over an area, A, determined by the geometry of the thruster (see Fig. 3). The mass flux for this model is given by

$$\Gamma = \frac{\dot{m}}{A}, \tag{11}$$

where $\dot{m}$ is the mass flow rate.

Because we are injecting our propellant through our cathode, the angle describing the divergence of the plume,

$$\theta = \tan^{-1}\left(\frac{r_a - r_c}{x}\right), \tag{12}$$

where r_a is the anode radius, r_c is the cathode radius, and x is the distance between the end of the cathode and the anode exit plane. The area of the surface at which the deposition takes place can then be found by integrating the resulting arc at distance d from the anode exit plane around the azimuthal axis, giving

$$A = 2\pi(1 - \cos\theta)(d + x)^2. \tag{13}$$

Using measurements of our thruster shown in Table 1, θ is found to be $18 \pm 2°$. Because of the size of the probe and its orientation, d has some variation that allows for a small range of possible plume areas. Over the entire probe, the theoretical mass flux found using this method and a 20 mg/s mass flow rate is 2.0 ± 0.4 µg/cm^2 s.

Parameter	Measurement
x	70 ± 1 mm
r_a	35 ± 1 mm
r_c	12.0 ± 0.5 mm
d	1.67 ± 0.03 m

Table 1. Measurements taken from the LiLFA.

C. Anticipated Measurement Error

In order to determine the mass flux, it is important to determine the time at which $t = 0$, corresponding to a bare probe for a given mass flux. This time differs from the time at which the band is first coated because it assumes a constant mass flux for the duration of the experiment, which is never possible since the mass deposition rate changes as a function of time for a short period until the thruster reaches steady state. Additionally, if the parameters of the thruster are changed while firing, resulting in an instantaneous change in Γ, the point at which $t = 0$ for the subsequent data will be unknown. In order to compensate for $t = 0$ being undefined, we modified Eq. 7 by replacing t with $t + t_c$, where t_c is a correction term. We were able to determine t_c by running a *for* loop through a range of values for t_c and minimizing the standard deviation between the average value for Γ and the calculated values at each point in time for a given period with a constant mass deposition rate. We assumed the deposition rate to be constant when all controllable parameters of the thruster were held constant at steady state operation.

Error in fitting a mass flux to data will vary depending on the duration over which data is taken at a constant mass deposition rate and on the amount of lithium already on the probe when the measurement is taken. Longer sample times provide a larger number of points to average. The measurement error increases as the resistance of the probe approaches the resistance of lithium. This is because once the probe has a lithium film of significant thickness, lithium deposition will not substantially change the voltage. As t becomes large, V decreases more slowly, eventually on the order of the noise in V.

The way in which lithium adheres to the stainless steel strip may change as a function of thickness, but after just 1 second of firing at 1 µg/cm^2 s, there are already $\mathcal{O}(10^5)$ monolayers of lithium on the probe, so this effect is assumed to be negligible in the timescales of interest.

Oxidation of lithium by residual gases can increase the resistance of lithium. In order for this effect to be minimal, the deposition rate of lithium must be much greater than the rate of oxidation of a surface of lithium. For our purposes, we use the data from Ref. 4 to determine that at 10^{-4} Torr, we will have on the order of a single monolayer of lithium oxide per second. This is equivalent to a mass flux of 8×10^{-3} µg/cm^2 s. If we wish to measure mass fluxes of this order, we must operate at lower pressures than 4×10^{-4} Torr in order to reduce the oxidation rate. Since we anticipate working in the 1 µg/cm^2 s regime, the effect of lithium oxidation is insignificant.

III. Experimental Apparatus

A. Facilities

All data was gathered at the Steady State Low Power (SSLP) facility in the Electric Propulsion and Plasma Dynamics Lab (EPPDyL) at Princeton University. The thruster in this facility is the LiLFA, which operates at up to 30 kW at steady state with applied field strengths up to 1600 G. The LiLFA is situated in a stainless steel vacuum chamber that is 1.5 m wide and 3.6 m long. Lithium is loaded into the feed system for the thruster under constant positive argon pressure to keep the lithium free of contamination. The vacuum chamber is then pumped down to an ultimate base pressure of about 2×10^{-5} Torr. We melt the lithium, and then pump it into the thruster using a mechanical piston. The lithium enters the thruster through a multichannel hollow cathode, where it is vaporized by a graphite heater. A detailed description of the feed system operation and lithium handling procedures can be found in Ref. 6, and an overview of our vacuum facilities and thruster can be found in Ref. 7.

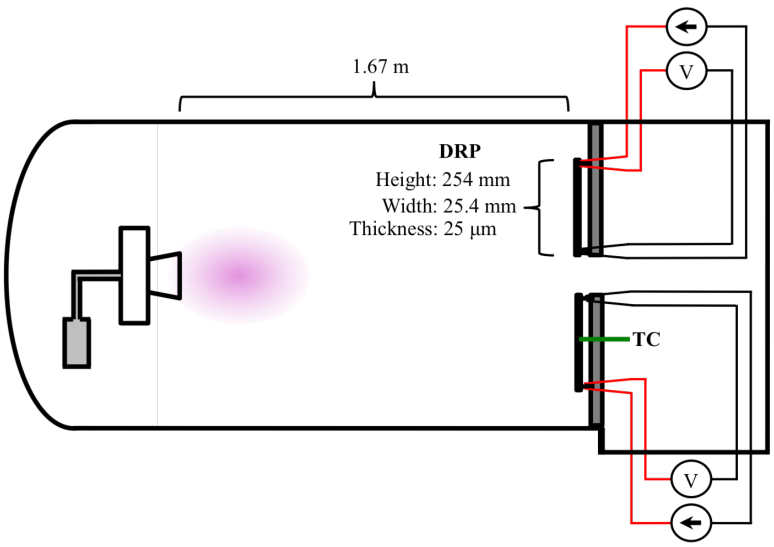

Figure 4. Cross-sectional diagram of the vacuum tank containing the lithium Lorentz force accelerator and diagnostics. The bottom probe was damaged by aluminum foil used to protect the vacuum tank, rendering the probe unusable.

B. Probe Detail

The present DRP is a 254 ± 3 mm strip of 304 stainless steel tape, which is 25.4 ± 0.1 mm wide and has a height of 25 ± 5 μm. The probe is situated 1.67 meters from the anode exit plane, where it extends radially from 10 cm above the thruster axis upward, as illustrated in Fig. 4. The probe is fixed to a narrow aluminum brace using insulating ceramic risers at each voltage terminal. A Kepco JQE 36-3M is used to provide a constant 2.8 A through the probe. The potential across the probe is measured using a National Instruments DAQ and recorded in Labview. All probe temperature measurements are made via a type K thermocouple positioned under the probe at what is approximately equivalent to the average radius of the probe from the thruster axis.

IV. Proof-of-Concept Test

The LiLFA was fired at a constant current of $J = 130$ A, with a constant applied field strength of $B_A = 1550$ G, and a mass flow rate of $\dot{m} = 20$ mg/s at background pressures below 4×10^{-5} Torr. The results of the first test of the DRP are presented in Fig. 5. The thruster is fired at approximately 60 seconds. As the arc is formed, there is substantial noise in the data until about 140 seconds. During the first 40 seconds of firing, it appears that a large quantity of lithium is deposited on the probe. Before the voltage was applied to the thruster, lithium was observed dripping from the cathode, so the initial ionization event utilized more lithium than would be available at steady state, resulting in the large deposit.

From 140 to 170 seconds, the slope of the data is uncharacteristically low, indicating a low rate of deposition on the probe. The cause for this aberration is unknown, but it is known that after the plasma is formed, heating in the thruster increases, which increases the vaporization rate of lithium until steady state is reached. It is possible then that an initial low mass flux was measured as the rate of vaporization and ionization was still increasing to steady state.

Fig. 5 shows the theoretical expectation for two different mass fluxes. 0.35 μg/cm^2 s agrees very well with the data from 170 to 440 seconds. The theoretical curve corresponding to 0.5 μg/cm^2 s is shown as a comparison, indicating the sensitivity of the measurement. The mass flux based on matching the theoretical model to the data is 0.35 ± 0.02 μg/cm^2 s, with the error based on the value at which 95% of the measured instantaneous Γ values were included. The calculated average mass flux and data are shown in Fig. 6.

The expected mass flux from Sec. II is 2.0 ± 0.4 μg/cm^2 s. During operation, however, the plume was photographed, and the angle θ was measured to be closer to 30°, rather than 18°, as shown in Fig. 7. Using this new value in Eqs. 13 and 11, the anticipated mass flux is then found to be 0.77 ± 0.02 μg/cm^2 s. This

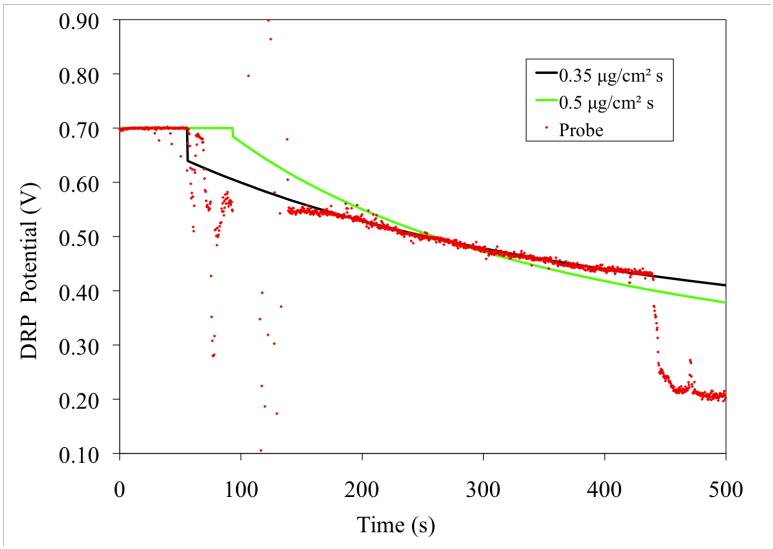

Figure 5. Potential across the DRP vs. time. The solid lines represent the theoretical values for two different mass fluxes. Measurements are shown in red. Firing starts at approx. 60 seconds. Data error is assumed to be on the order of the measurement during the initial plasma formation. At 170 seconds, steady state operation is assumed to begin. The measured value of 0.35 ± 0.02 µg/cm^2 s was made between 170 seconds to 440 seconds, where the data noise error is ± 0.01 V.

estimation is still more than twice as large as the measured quantity. This is expected for two reasons. First, although there is a defined cutoff where the angle θ is illustrated, a small fraction of the plume can be observed beyond this angle. Second, we do not expect all of the lithium impinging upon the DRP to adhere to it since condensible propellant backscatter has been observed even with cryogenically cooled chamber walls.[2] For this reason, our measurement is indicative of a deposition rate corresponding to a lower bounds of the mass flux in the plume.

An additional source of deviation from the expected mass flux value is that the plume radius spanned by the probe extends from near the thruster axis to 12.9° off axis. It is expected that the plume has a density distribution that is a function of the angle with the thruster axis. This distribution would need to be known in order to determine the resistivity of the DRP as a function of distance along the length of the probe. As a result, we have measured the average mass flux along the length of the probe. Future experiments can avoid this source of error by using an arc shaped probe situated at a constant radius from the thruster axis.

Our model ceases to describe the data in Fig. 5 at 440 seconds, where the voltage across the probe drops sharply. The most plausible explanation for this drop is that lithium coated the ceramic risers intended to keep the probe insulated from the aluminum brace, significantly reducing the resistance between the terminals. This is not testable after venting our vacuum chamber because the lithium coating the surface of the probe and risers has reacted with water during our neutralization process to form lithium hydroxide, which is nonconductive. This can, fortunately, be mitigated in the future, by attaching a secondary cylinder around each ceramic riser, connected only to the brace. This would shield enough of the riser to prevent the lithium from creating a bridge to the brace. This is illustrated in Fig. 8.

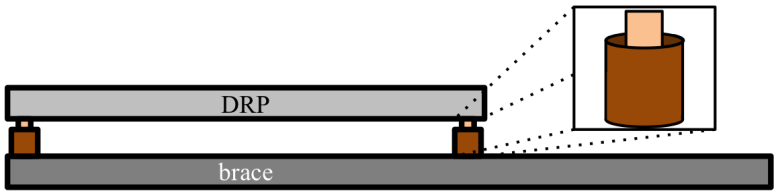

Figure 8. Diagram illustrating how a cylindrical shell around the ceramic riser holding the DRP in place can be used to prevent lithium from bridging the DRP to the brace.

With regards to the nondimensional parameter $\bar{\Gamma}$, the temperature data presented in Fig. 9 show that

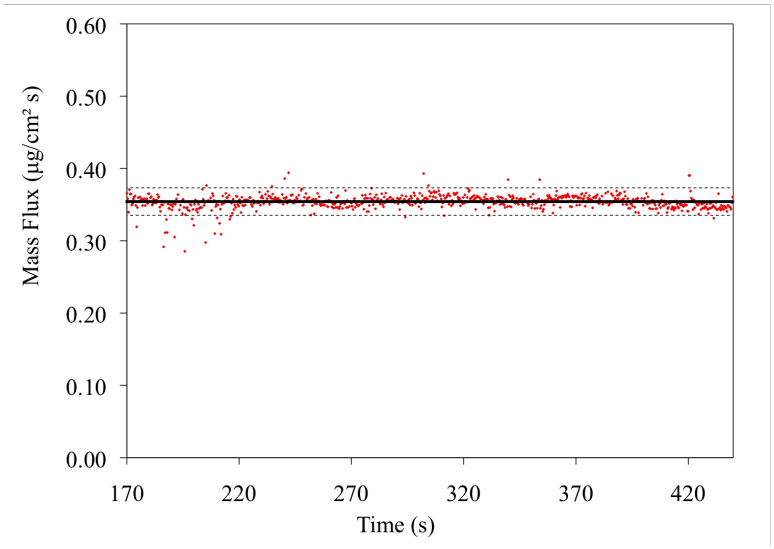

Figure 6. Mass flux vs. time. The solid line represents the average of the calculated data points, which are shown in red. The average propagated error for the instantaneous Γ values is 13 ng/cm^2 s. The dotted lines represent the values around the average mass flux within which 95% of data points reside. The mass flux is found to be 0.35 ± 0.02 μg/cm^2 s.

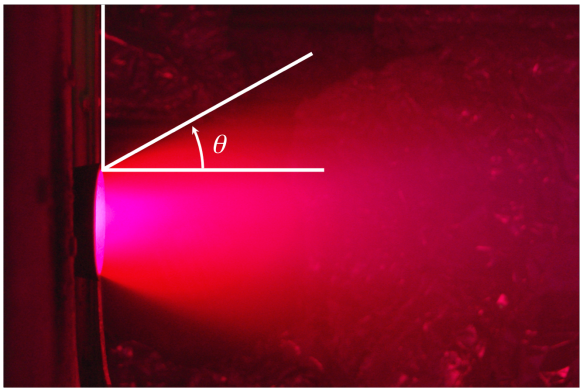

Figure 7. Approximate measurement of plume divergence for estimation of mass flux.

the temperature never exceeds the melting temperature of lithium during this experiment. However, the temperature was still increasing when the data became unusable at 440 seconds. If the temperature had reached the melting temperature of lithium (180° C), $\bar{\Gamma}$ would have reached unity in ~ 6 s, and the flow of lithium off the probe would need to be modeled.

V. Conclusion

The dynamic resistance probe was presented as a new diagnostic capable of measuring the deposition rate of condensible and conductive propellant. A theoretical model was developed to predict the behavior of the potential across this probe, which was found to be dependent on mass deposition rate, temperature, and probe exposure time. As the latter two of these variables are easily measured, the DRP is an effective tool in measuring mass deposition rate. A prototype was constructed and tested with the LiLFA and the test showed excellent agreement with the theoretical model.

Differences between measured and predicted deposition rate are expected to be due to excessive plume divergence and propellant backscatter from the probe. The first test of the DRP demonstrated a data scatter of 6% around the measured mass flux, a substantial step forward from previous measurements using QCM

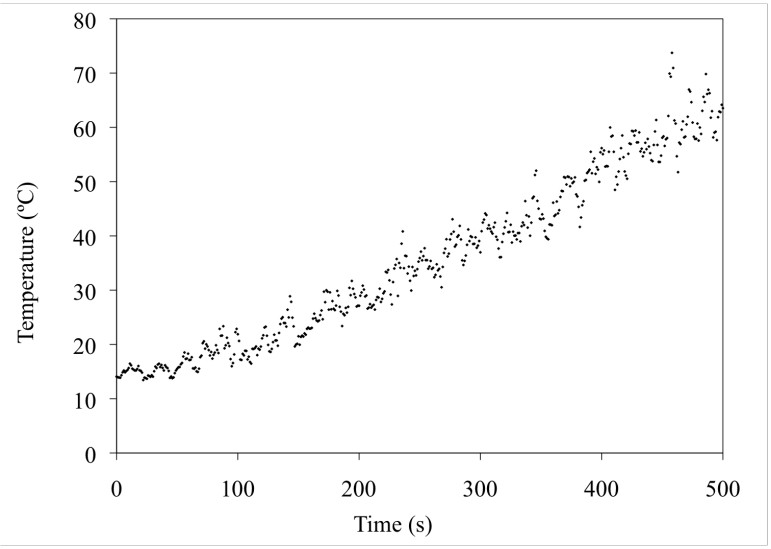

Figure 9. Temperature measured by a K-type thermocouple vs. time. Temperature data were recorded at 10 samples/second. Data points shown are smoothed by averaging over the twenty previous and twenty subsequent data points.

with the LiLFA, which had data scatter of 20%.[10]

Following our proof-of-concept test, we are planning additional experiments to confirm the success of the DRP. We will use active cooling of the probe to simplify the theoretical model and prevent lithium from running off the probe on subsequent tests. We will also begin using arc-shaped probes at fixed radii from the thruster axis to reduce the range of deposition rates across a single probe. The DRP has been proposed as a tool that could be used to measure deposition rates upstream of a thruster. The experimental evidence from this first test indicates measurements of low rates of deposition are feasible, and we plan to verify this by testing a DRP in situ in the plane parallel to the solenoid of the LiLFA.

Acknowledgments

We are grateful to Bob Sorenson for his technical assistance and to Dan Lev, who provided guidance based on his prior experience with the LiLFA.

References

[1]Little, J. M., and Choueiri, E. Y., "Influence of the Applied Magnetic Field Strength on Flow Collimation in Magnetic Nozzles," In 50th AIAA Joint Propulsion Conference, Cleveland, OH, USA, 28-30 July 2014. AIAA-2014-3912.

[2]Rudolph, L. K., Pless, L. C., and Harstad, K. G., "Pulsed Plasma Thruster Backflow Characteristics," In 15th AIAA/ASME/SAE Joint Propulsion Conference, Las Vegas, NV, USA, 18-20 June 1979. AIAA-79-1293.

[3]Kodys, A., and Choueiri, E., "A Critical Review of the State-of-the-Art in the Performance of Applied-Field Magnetoplasmadynamic Thrusters." AIAA-2005-4247, 2005.

[4]Skinner, C. H. et al., J. Nucl. Mater. (2013), http://dx.doi.org/10.1016/j.jnucmat.2013.01.136

[5]Ahmed, L. N., and Crofton, M. W., "Surface Modification Measurements in the T5 Ion Thruster Plume," Journal of Propulsion and Power, 14(3):336?347, May-June 1998.

[6]Kodys, A., et al., "Lithium Mass Flow Control for High Power Lorentz Force Accelerators," Space Technology and Applications International Forum, Albuquerque, NM, USA, February 2001, STAIF Paper 195.

[7]Lev, D. R., and Choueiri, E. Y., "Scaling of Efficiency with Applied Magnetic Field in Magnetoplasmadynamic Thrusters," Journal of Propulsion and Power, 28(3):609?616, May-June 2012.

[8]Chi, T. C., "Electrical Resistivity of Alkali Elements," *J. Phys. Chem. Ref. Data*, Vol. 8, No. 2, 1979.

[9]Ho, C. Y., and Chu, T. K., "Electrical Resistivity and Thermal Conductivity of Nine Selected AISI Stainless Steels," Cindas Report 45, Prepared for American Iron and Steel Institute, September 1977.

[10]Krämer, T., "3-D Characterization of the Plume of a Lithium Lorentz Force Accelerator (LiLFA)," Masters Thesis, Mechanical and Aerospace Engineering Dept., Universität Stuttgart, Germany, 2003.

[11]Lide, D. R., *CRC Handbook of Chemistry and Physics*, 77th ed., Boca Raton, FL. CRC Press, 1997. Page **6**-221.

[12]White, F. M., *Viscous Fluid Flow*, 2nd ed., Boston, MA. McGraw Hill, 1991. Pages 104-217.